Material Sciences Revista Mexicana de Física **71** 041006 1–14 JULY-AUGUST 2025

Structural and optoelectronic properties of rocksalt magnesium cadmium oxygen ternary alloys: For ultraviolet applications

N. Hassani
Materials Laboratory, Research Center (CFTE), Sidi Bel Abbs Djillali Liabes University, 22000, Algeria,
Electronic Department, University Djillali Liabes of Sidi Bel Abbes, 22000 Sidi Bel Abbes, Algeria.

M. Benchehima
Electronic Department, University Djillali Liabes of Sidi Bel Abbes, 22000 Sidi Bel Abbes, Algeria,
Electronic Department University of Sciences and Technology of Oran, Mohamed Boudiaf (USTO), El M'nouar BP 1505, Oran, Algeria,
e-mail:mbenchehima@yahoo.fr; miloud.benchehima@univ-usto.dz

H. Abid
Materials Laboratory, Research Center (CFTE), Sidi Bel Abbs Djillali Liabes University, 22000, Algeria,
Electronic Department, University Djillali Liabes of Sidi Bel Abbes, 22000 Sidi Bel Abbes, Algeria.

Received 1 December 2024; accepted 16 February 2025

In this work, we present a comprehensive investigation regarding the physical properties of $\mathrm{Mg}_x\mathrm{Cd}_{1-x}\mathrm{O}$ ternary alloys for different concentrations ($0 \leq x \leq 1$), in rock salt phase. These properties, including structural, electronic, and optical properties, were studied using the full-potential linearized augmented plane wave (FP-LAPW) method based on the density functional theory (DFT) with the Wien2k code. The structural parameters of rock salt $\mathrm{Mg}_x\mathrm{Cd}_{1-x}\mathrm{O}$ are studied in detail as a function of Mg concentration using the generalized gradient approximation developed by Perdew-Burke-Ernzerhof for solids (GGA-PBEsol). The calculated structural parameters of both binaries are in good agreement with their corresponding theoretical and experimental data. The results show that the value of the lattice parameter of rock salt $\mathrm{Mg}_x\mathrm{Cd}_{1-x}\mathrm{O}$ decreases almost linearly with the increasing Mg concentration and exhibits a small deviation from the linear composition dependence (LCD). Both local density approximation (LDA) and Tran-Blaha modified Becke-Johnson approximation (TB-mBJ) were used to explore the electronic properties. It is found that the increasing Mg concentration leads to increasing energy band gap. Our obtained results demonstrate that the rock salt CdO has an indirect band gaps and rock salt MgO has a direct band gap, while $\mathrm{Mg}_x\mathrm{Cd}_{1-x}\mathrm{O}$ ternaries ($0.125 \leq x \leq 0.875$) exhibit an indirect band gap semiconductors. Additionally, the linear optical properties, including complex dielectric function, complex refractive index, absorption coefficient and optical conductivity, are calculated and discussed in detail. The obtained results confirm that the rock salt $\mathrm{Mg}_x\mathrm{Cd}_{1-x}\mathrm{O}$ ternary alloys are a promising candidate for ultraviolet photo electronic devices.

Keywords: Cadmium oxide; magnesium oxide; super cell; complex dielectric function; optical conductivity; WIEN2k simulation software.

DOI: https://doi.org/10.31349/RevMexFis.71.041006

1. Introduction

II-VI semiconductor materials and their heterostructures have been of growing interests because of their interesting physical properties and their potential application in the field of optoelectronics [1–5]. These materials are also called wide band gap semiconductors. These semiconductor compounds appear to be perfect candidates for use in solar cells [6], light-emitting diodes [7], displays [8], nonlinear optics and used in solid-state tunable lasers [1]. Among these materials, we mention the cadmium oxide (CdO) and magnesium oxide (MgO), which have been the subject of numerous theoretical and experimental studies [9–14]. Magnesium oxide (MgO) with direct band gap energy of 7.8 eV [15] is considered as a promising material for optical window application [16, 17]. Magnesium oxide is utilized in the alternating current-plasma display panel due to its physical stability, high transmittance, and high secondary electron emission [9, 18]. In addition, MgO binary compound is considered to be a transparent dielectric material [10, 13]. While, the cadmium oxide (CdO) is indirect band gap equal to 1.35 eV [19]. CdO has unique characteristics of high conductivity and high transmission, which made it applicable in many devices such as photodiodes, phototransistors, photovoltaics, transparent electrodes, liquid crystal displays, smart windows, optical communications and anti-reflecting coatings [9,10,20,21]. Under normal conditions, both binaries (CdO and MgO) crystallize in rock salt (RS) phase with the space group ($Fm\bar{3}m$) [22]. By combining the two materials CdO and MgO, we can obtain the mixed $\mathrm{Mg}_x\mathrm{Cd}_{1-x}\mathrm{O}$ ternaries. In recent years, various properties of $\mathrm{Mg}_x\mathrm{Cd}_{1-x}\mathrm{O}$ ternary have been investigated both experimentally and theoretically. Paliwal *et al.* [23] and Amin *et al*. [9] investigated the structural, electronic and optical properties of $\mathrm{Mg}_x\mathrm{Cd}_{1-x}\mathrm{O}$ ($0 \leq x \leq 1$) in rocksalt phase using the first-principle method. Stability, structural phase transition and electronic properties of $\mathrm{Mg}_x\mathrm{Cd}_{1-x}\mathrm{O}$ have been investigated using the linear combination of atomic orbitals (LCAO) method within the framework of the density functional theory by Joshi *et al*. [24]. Electronic and optical properties of $Mg_xCd_{1-x}O$ ternary alloys have also been recently investigated by Djaili *et al*. [10] using the full potential linearized augmented plane wave (FP-LAPW) method. In order to describe the disordered $Mg_xCd_{1-x}O$ ternary alloys, they have used 8-atoms special quasi-random structures (SQS). They have calculated the structural of $Mg_xCd_{1-x}O$ ternaries using the generalized gradient approximation of Wu and Cohen (GGA-WC) [25]. For the electronic and optical properties, they have employed the Tran-Blaha modified Becke-Johnson approximation (TB-mBJ) [26]. In the present work, we aimed to provide some additional complementary information to the existing data on the disorder effect of ternaries ($x = 0$, 0.125, 0.250, 0.375, 0.500, 0.625, 0.750, 0.875 and 1), in rock salt phase, using the full potential linearized augmented plane wave (FP-LAPW) [27]. In the present calculation, a 16-atom simple cubic supercell based on the special quasi-random structure (SQS) approach of Zunger *et al.* [24] is adopted to model the considered $Mg_xCd_{1-x}O$ ternary alloys. We have calculated the structural properties and cohesive energy by means of (GGA-BPESol) approach [28]. Electronic and optical properties of $Mg_xCd_{1-x}O$ ternaries were calculated using the local density approximation (LDA) [29, 30] and the modified Becke-Johnson (TB-mBJ) [31] approaches. We are motivated by the fact that there are few studies available on the physical properties of RS $Mg_xCd_{1-x}O$ ternary alloys. So, the aim of this work is to complete the works initiated by Amin *et al*. [9], Djaili *et al*. [10] and Paliwal *et al.* [23] and to collect a lot of information of theses ternary alloys, providing a global understanding of RS $Mg_xCd_{1-x}O$ ternaries and their main characteristics, which could offer interesting perspectives for their use in solar cells and optoelectronic devices. Our obtained results are compared to existing data in the literature. The paper is organized as follows: Section 2 describes the computational methods used. Section 3 presents and discusses results on structural and optoelectronic properties of RS $Mg_xCd_{1-x}O$ ternary alloys and their end binaries (CdO and MgO). Section 4 summarizes the findings.

2. Computational method

The calculations in this research were carried out via the full potential linearized augmented plane wave (FP-LAPW) formalism, grounded in density functional theory (DFT) [32], using the computational code Wien2k [33]. For the exchange-correlation potential, the generalized gradient approximation proposed by Perdew-Burke-Ernzerhof for solids (GGA-BPESol) [28] was employed only for calculating the fundamental structural properties. The local density approximation (LDA) [29, 30] and the modified Becke-Johnson (TB-mBJ) [31] were applied to calculate the electronic properties of RS $Mg_xCd_{1-x}O$ ternary alloys. For the computation details, the muffin tin radii (R_{MT}) values for Mg, Cd and O atoms are selected as 1.9 $(a.u)^{-1}$, 2.1 $(a.u)^{-1}$ and 1.9 $(a.u)^{-1}$, respectively. To attain convergence of energy eigenvalues, the wave function in interstitial regions was expanded in the plane wave with a cut off of $R_{MT}K_{\max} = 8$. ($K_{\max}$ is the magnitude of the largest vector K in the plane wave expansion). The energy gap between the core and valence bands was taken equal to -6 Ry. The valence wave functions inside the spheres ($l_{\max}$) and the charge density ($G_{\max}$) were expanded up to 10 and 12, respectively. To obtain better results, the self consistent calculations were considered to have converged when the total energy of the system is stable with 10^{-4} Ryd 10^{-4} Ryd. In order to simulate the $Mg_xCd_{1-x}O$ ternary alloys, in rock salt structure, we used cubic supercell

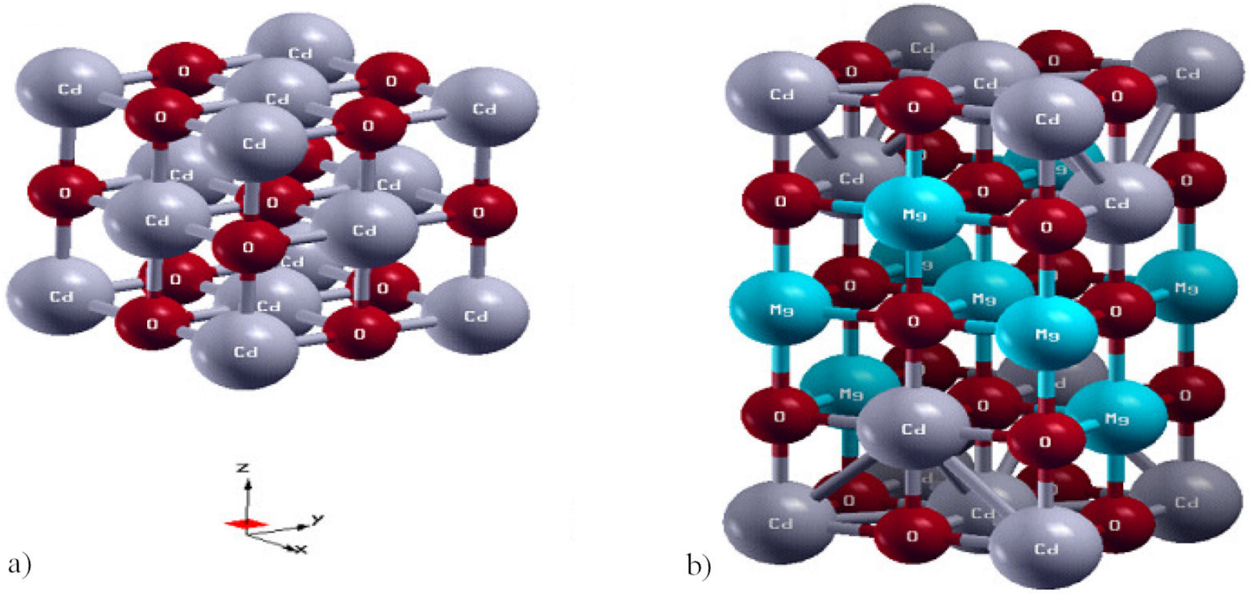

FIGURE 1. Crystal structure of a) CdO (primitive cell) and b) $Mg_{0.500}Cd_{0.500}O$ (supercell), in rocksalt structure.

contemning 16 atoms that corresponds ($10 \times 10 \times 5$) conventional cell based on the special quasi random structure approach of Zunger *et al*. [34]. For well convergence of energy, we used 108 k-points ($12 \times 12 \times 6$ mesh grid) in the integration over the irreducible Brillouin zone for binary the ternaries. For the optical properties calculations, we have increased the number of points in the irreducible part of the Brillouin zone (BZ) to 196 k-points ($12 \times 12 \times 6$ mesh grid). In the pseudo atomic calculations, the Mg: [Ne] $3s^2$, Cd: [Kr] $4d^{10}5s^2$ and O: [He] $2s^2 2p^4$ electron states were treated as valence states. The crystal structure of CdO binary (primitive cell) and $\mathrm{Mg}_{0.500}\mathrm{Cd}_{0.500}\mathrm{O}$ ternary (supercell), in rock salt structure are shown in Fig. 1.

3. Results and discussion

3.1. Structural properties and cohesive energy

At room temperature, the most stable structure for CdO and MgO binary compounds is the rock salt phase with space group ($Fm\bar{3}m$) [22]. Due to the small difference in lattice parameters between CdO and MgO binaries, we assume that their $\mathrm{Mg}_x\mathrm{Cd}_{1-x}\mathrm{O}$ ternary alloys retain the rock salt phase. Therefore, the rock salt phase is adopted for $\mathrm{Mg}_x\mathrm{Cd}_{1-x}\mathrm{O}$ ternary alloys to investigate their ground state properties. Structural parameters, such as lattice constant and bulk modulus, are calculated using the (GGA-PBESol) approach [35] based on Murnaghan's equation of state (EOS) [36],

$$E(V) = E_0 + \frac{B_0 V}{B_0'} \left(\frac{\left(\frac{V_0}{V}\right)^{B_0'}}{B_0' - 1} + 1 \right) - \frac{B_0 V}{B_0' - 1}, \quad (1)$$

where E_0 represents the equilibrium energy, B_0 and B_0' represent the bulk modulus and the pressure derivative of bulk modulus, respectively. Table I summarizes the optimized structural parameters of $\mathrm{Mg}_x\mathrm{Cd}_{1-x}\mathrm{O}$ for ($0 \leq x \leq 1$), in rock salt, compared to available experimental and theoretical data. The calculated lattice constants of CdO and MgO are 4.7001 Å and 4.2187 Å, which are good agreement with the experimental data (4.686 Å for CdO [15] and 4.203 Å for MgO [15]). We can note that the small difference between the calculated and experimental values can be attributed to the general trend that (GGA-BPESol) generally overestimates these parameters. Furthermore, it is observed that the calculated lattice parameters of both binaries are in excellent agreement with their corresponding theoretical results using the same approach given in Refs. [9, 10]. Moreover, the calculated bulk modulus values of CdO and MgO are 148.266 GPa and 155.1853 GPa, respectively. These values are in good agreement with the experimental values given in Refs. [37, 38]. The optimized structural lattice constant (a) and bulk modulus (B) of $\mathrm{Mg}_x\mathrm{Cd}_{1-x}\mathrm{O}$ in rock salt phase at some selected Mg concentrations ($x = 0$, 0.125, 0.250, 0.375, 0.500, 0.625, 0.750, 0.875 and 1) are listed in Table I. A small difference was observed between our calculated results and those reported in Refs. [9, 10]. According to Vigard's law [15], the lattice constants for $\mathrm{Mg}_x\mathrm{Cd}_{1-x}\mathrm{O}$ ternary alloys as a function of Mg concentration can be estimated as follows:

$$a_{\mathrm{Mg}_x\mathrm{Cd}_{1-x}\mathrm{O}}(x) = x a_{\mathrm{MgO}} + (1-x) a_{\mathrm{CdO}}. \quad (2)$$

Here,a_{MgO} and a_{CdO} are the lattice constants for the end binaries MgO and CdO, respectively. Figure 2 presents the variation of the lattice constants $a(x)$ and the bulk modulus B(x) as a function of magnesium concentrations for $\mathrm{Mg}_x\mathrm{Cd}_{1-x}\mathrm{O}$ ternary alloys in rock salt structure. From the results, we may observe that the lattice constant of $\mathrm{Mg}_x\mathrm{Cd}_{1-x}\mathrm{O}$ decreases with the increase of Mg concentration. This is due to the lower size of the replaced magnesium

TABLE I. Calculated lattice constant a(Å), bulk modulus B(GaP) and cohesive energy $E_{\mathrm{Coh}}(Ry)$ of RS $\mathrm{Mg}_x\mathrm{Cd}_{1-x}\mathrm{O}$ ternary alloys using (GGA-PBESol) approach.

$\mathrm{Mg}_x\mathrm{Cd}_{1-x}\mathrm{O}$	Present work (GGA-BPESol)			Other calculations		Experiment	
	a(Å)	B(GaP)	$E_{\mathrm{Coh}}(Ry)$	a(Å)	B(GPa)	a(Å)	B(GPa)
CdO	4.7001	148.266	-8.771	4.77 [9], 4.696 [10]	123.599 [9]	4.686 [15]	148 [37]
$\mathrm{Mg}_{0.125}\mathrm{Cd}_{0.875}\mathrm{O}$	4.6576	147.0659	-332.366				
$\mathrm{Mg}_{0.250}\mathrm{Cd}_{0.750}\mathrm{O}$	4.61765	147.6271	-332.376	4.68 [9] , 4.611 [10]	130.374 [9]		
$\mathrm{Mg}_{0.375}\mathrm{Cd}_{0.625}\mathrm{O}$	4.5730	148.3949	-332.386				
$\mathrm{Mg}_{0.500}\mathrm{Cd}_{0.500}\mathrm{O}$	4.5229	149.8635	-332.396	4.57 [9] , 4.523 [10]	133.966 [9]		
$\mathrm{Mg}_{0.625}\mathrm{Cd}_{0.375}\mathrm{O}$	4.4652	151.5759	-332.406				
$\mathrm{Mg}_{0.750}\mathrm{Cd}_{0.250}\mathrm{O}$	4.3985	153.3266	-332.417	4.44 [9] , 4.394 [10]	139.659 [9]		
$\mathrm{Mg}_{0.875}\mathrm{Cd}_{0.125}\mathrm{O}$	4.3205	156.4442	-332.427				
MgO	4.2187	157.1823	-8.90611	4.26 [9], 4.220 [10]	146.6281 [9]	4.203 [15]	156 [38]

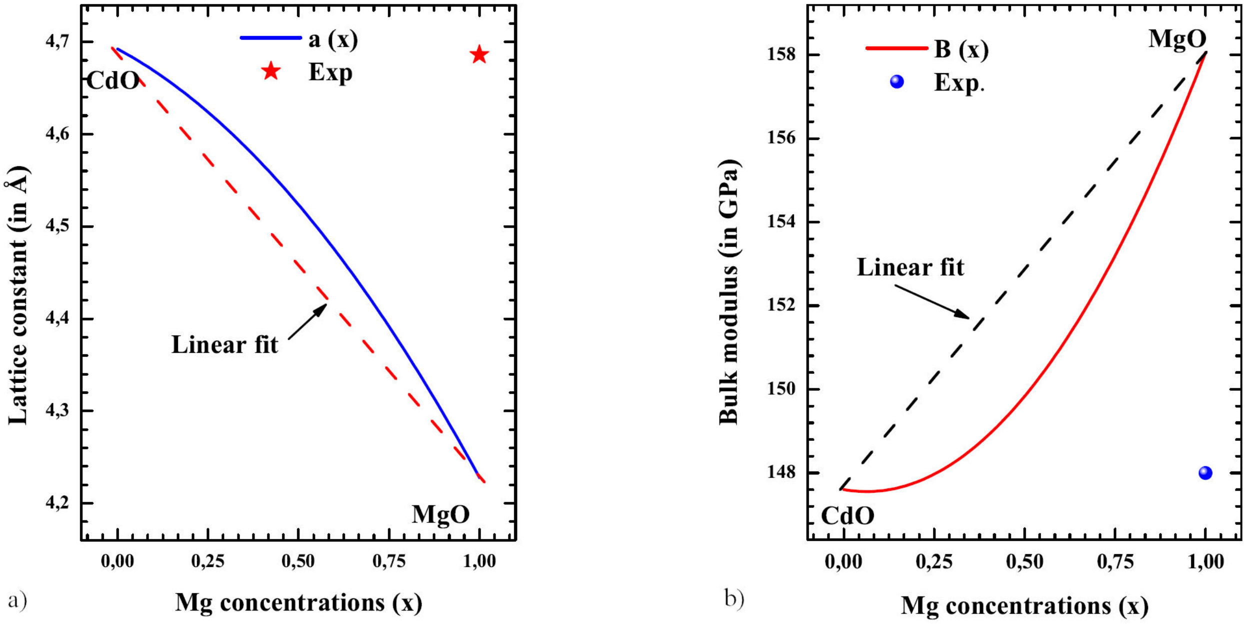

a) b)

FIGURE 2. Lattice constants $a(x)$ and bulk modulus $B(x)$ as a function of Mg concentrations for $\mathrm{Mg}_x\mathrm{Cd}_{1-x}\mathrm{O}$ ternary alloys in rock salt structure.

(Mg) atoms comparing to host cadmium (Cd) atoms. Furthermore, it is observed that B(x)'s values increase as the magnesium composition increases. This suggests that as Mg increases from $x = 0$ (CdO), to $x = 1$ (MgO), $\mathrm{Mg}_x\mathrm{Cd}_{1-x}\mathrm{O}$ becomes generally more compressible. The total bowing parameters of lattice constant (b_a) and bulk modulus (b_B) were obtained, by fitting the calculated values of $a(x)$ and $B(x)$ to the quadratic polynomial function:

$$a_{\mathrm{Mg}_x\mathrm{Cd}_{1-x}\mathrm{O}}(x) = 4.9623 - 0.2105x - 0.2537x^2, \quad (3)$$

$$B_{\mathrm{Mg}_x\mathrm{Cd}_{1-x}\mathrm{O}}(x) = 147.6026 - 1.5165x + 11.9691x^2. \quad (4)$$

Our calculated total bowing parameters are found to be $b_a = -0.2537$ Å and $b_B = 11.9691$ GPa for lattice constant and bulk modulus, respectively. From Fig. 2, we can see that the decrease in the lattice constant of $\mathrm{Mg}_x\mathrm{Cd}_{1-x}\mathrm{O}$ ternary alloys is accompanied by an increase the bulk modulus. This finding shows that the bulk modulus is in inverse sequence to the lattice constant which is in agreement with the well-known relationship (inverse) between B and a, $B\alpha V^{-1}$ [39]. It can be noted that Eqs. (3) and (4) can be used as models to determine the lattice constant value and bulk modulus of $\mathrm{Mg}_x\mathrm{Cd}_{1-x}\mathrm{O}$ ternary alloys for different magnesium compositions x ($0 \leq x \leq 1$), respectively. The cohesive energy (E_{Coh}) is then the difference between the total energy of the isolated atoms and the total energy of material. Cohesive energy also reveals the strength and robustness of internal atomic bonds. In order to study the structural stability of $\mathrm{Mg}_x\mathrm{Cd}_{1-x}\mathrm{O}$ ternary alloys in ordered form, we calculated the cohesive energy (E_{Coh}) of the nine structures ($n = 0$, 1, 2, 3, 4, 5, 6, 7 and 8) using the following relation [40]:

$$E_{\mathrm{Coh}}^{\mathrm{Mg}_x\mathrm{Cd}_{1-x}\mathrm{O}} = \frac{E_{\mathrm{Total}}^{\mathrm{Mg}_x\mathrm{Cd}_{1-x}\mathrm{O}} - \left(n_1 E^{\mathrm{Mg}} + n_2 E^{\mathrm{Cd}} + n_3 E^{\mathrm{O}}\right)}{n_1 + n_2 + n_3}. \quad (5)$$

Here, $E_{\mathrm{Total}}^{\mathrm{Mg}_x\mathrm{Cd}_{1-x}\mathrm{O}}$ denotes the total energy of the supercell. n_1, n_2 and n_3 are the number of Mg, Cd and O atoms in $\mathrm{Mg}_x\mathrm{Cd}_{1-x}\mathrm{O}$ supercell structure, respectively. E^{Mg}, E^{Cd} and E^{O} are the total energies of the isolated atoms of magnesium (Mg) cadmium (Cd) and oxygen (O), respectively. The total energy of the isolated atom was evaluated by considering at a supercell containing an isolated atom.

The calculated cohesive energy values for $\mathrm{Mg}_x\mathrm{Cd}_{1-x}\mathrm{O}$ ternary alloys in rock salt structure are listed in Table I. According to the results reported in Table I, the cohesive energies of all $\mathrm{Mg}_x\mathrm{Cd}_{1-x}\mathrm{O}$ ternaries are negative, confiring their structural stability.

3.2. Electronic properties

3.2.1. *Band structures and bowing parameter*

In this section, we calculated the band structures of $\mathrm{Mg}_x\mathrm{Cd}_{1-x}\mathrm{O}$ ternary alloys and their end binaries along the high symmetry directions in the first Brillouin zone by using the predicted lattice parameter within (WC-PBESol) approach. These properties were computed using local density approximation (LDA) [29, 30] and the semi local functional of Tran and Blaha (TB-mBJ) [31] approaches. The reference of energy level is taken as the peak of the valence band. Our calculated values of energy gap (E_g) of RS $\mathrm{Mg}_x\mathrm{Cd}_{1-x}\mathrm{O}$ ternaries obtained by (LDA) and (TB-mBJ) are presented in Table II. It was observed that the pattern of the calculated

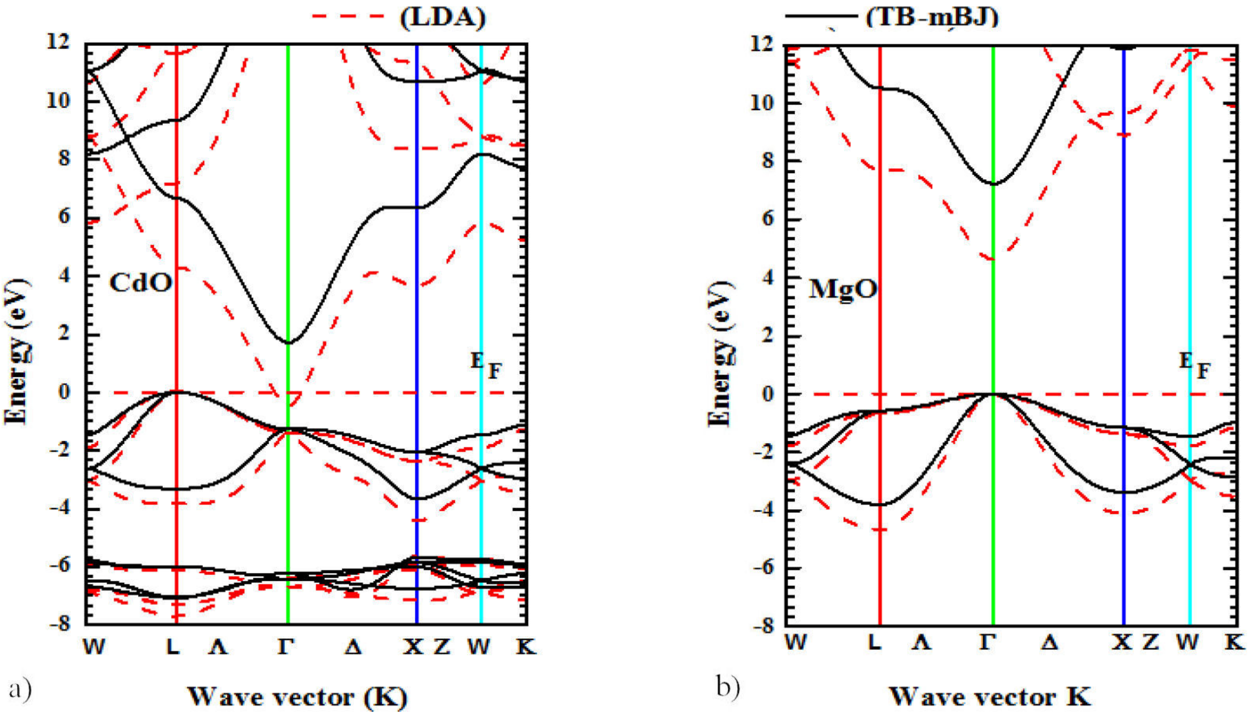

FIGURE 3. Energy band structures of RS CdO and RS MgO calculated with (LDA) and (TB-mBJ) approaches.

TABLE II. Calculated values of energy gap (E_g) of RS $Mg_xCd_{1-x}O$ ternaries, using (LDA) and (TB-mBJ) approaches.

Material	Energy band gap E_g (in eV)					
		This work		Other calculations		
	Type of band gap	LDA	TB-mBJ	GGA	TB-mBJ	Experiment
CdO	$(X-\Gamma)$	-0.51863	1.586	-0.5 [9]	1.81 [10]	2.16 [15]
$Mg_{0.125}Cd_{0.875}O$	$(M-\Gamma)$	-0.329	1.767			
$Mg_{0.250}Cd_{0.750}O$	$(M-\Gamma)$	-0.088	1.992	-0.2 [9]	2.26 [10]	
$Mg_{0.375}Cd_{0.625}O$	$(M-\Gamma)$	0.195	2.246			
$Mg_{0.500}Cd_{0.500}O$	$(M-\Gamma)$	0.520	2.588	0.5 [9]	2.76 [10]	
$Mg_{0.625}Cd_{0.375}O$	$(M-\Gamma)$	0.820	2.927			
$Mg_{0.750}Cd_{0.250}O$	$(M-\Gamma)$	1.175	3.330	1.1 [9]	3.71 [10]	
$Mg_{0.875}Cd_{0.125}O$	$(M-\Gamma)$	1.605	3.817			
MgO	$(\Gamma-\Gamma)$	4.605	7.175	4.6 [9], 4.70 [41]	7.39 [10], 7.17 [41]	7.8 [15]

band structures of these materials is similar for both approximations and the main difference is in the values of the energy band gap (E_g). In order to depict the difference in band gap values, we present the electronic band structures of RS CdO and RS MgO together obtained via (LDA) and (TB-mBJ) approaches in Fig. 3. The peak of the valence band was positioned on the zero-energy Fermi level (E_F). The result obtained via the two approximations (LDA) and (TB-mBJ) indicates that RS CdO binary compound has an indirect band gap along ($L-\Gamma$) while RS MgO has a direct band gap along ($\Gamma-\Gamma$), which is in good agreement with the available data given in Refs. [9, 10, 15, 41]. Moreover, the calculated band gaps values of RS CdO and RS MgO binaries presented in Table II agree well with other theoretical results using the same approaches. And, it was observed the band gap values obtained by (LDA) approach are underestimated compared to the experimental data. This can be attributed to the limitation of (LDA) within density functional theory (DFT) [41]. (TB-mBJ) gave band gap values of 1.586 eV and 7.175 eV for RS CdO and RS MgO, respectively, which are much closer to their corresponding experimental values (see Table II). Due to the similar behavior observed in the calculated band structures across both approaches, we presented only the electronic band structures obtained from (TB-mBJ)

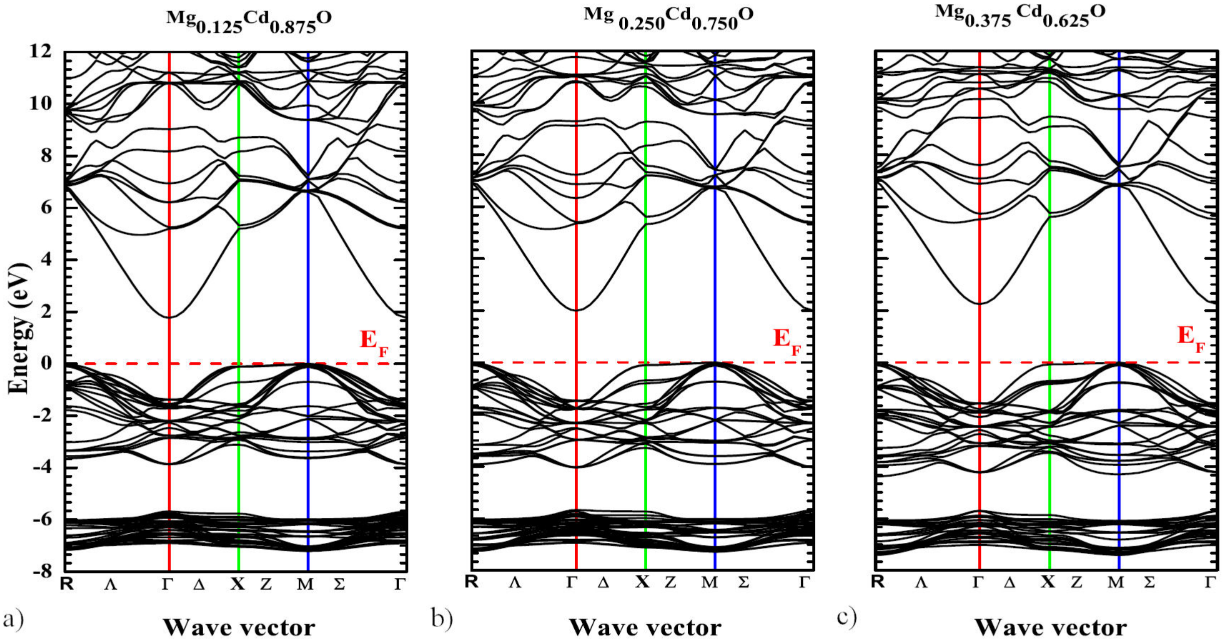

FIGURE 4. Energy band structures of $Mg_{0.125}Cd_{0.875}O$, $Mg_{0.250}Cd_{0.750}O$ and $Mg_{0.375}Cd_{0.625}O$ calculated with (TB-mBJ) approach, in rock salt phase.

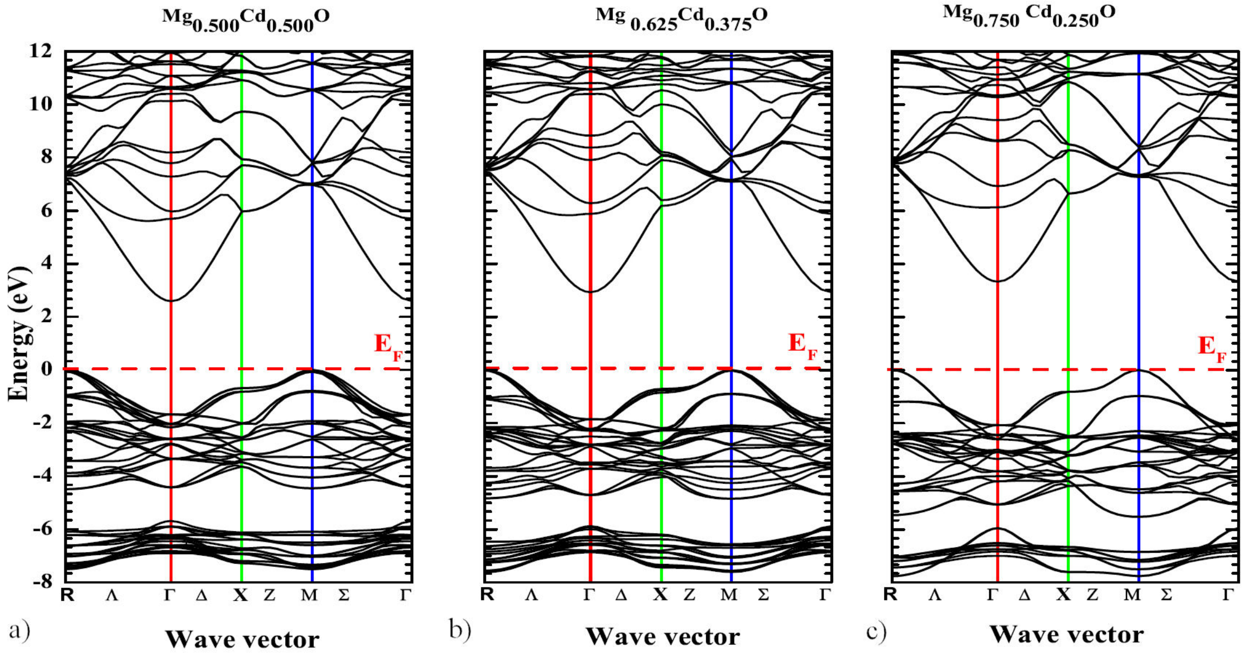

FIGURE 5. Energy band structures of $Mg_{0.500}Cd_{0.500}O$, $Mg_{0.625}Cd_{0.375}O$ and $Mg_{0.750}Cd_{0.250}O$ calculated with(TB-mBJ) approach, in rock salt phase.

approach in Figs. 4-5 for concentrations ($x = 0.125$, 0.25, 0.375, 0.500, 0.625 and 0.75). For all considered concentrations, our investigations show that the (valence band maximum) $BV_{\max}$ occurs at M point and the (conduction band minimum) $BC_{\min}$ is found at Γ point, indicating that these ternaries are indirect band gap at $(M - \Gamma)$, which agrees well with previous theoretical studies given in Refs [9, 10].

3.2.2. *Densities of states*

In this section, we have calculated and discussed the electronic density of states (DOS) of $Mg_xCd_{1-x}O$ ternary alloys, in rock salt structure. The knowledge of the (DOS) facilitates the analysis of the electronic and optical properties of the semiconductor materials [43]. The total density of states (TDOS) with the partial density of states (PDOS) were calcu-

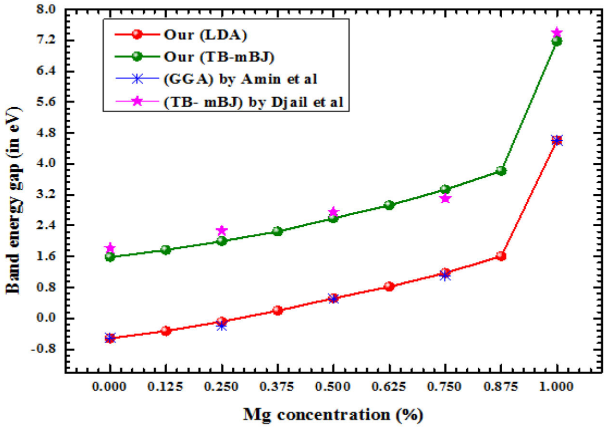

FIGURE 6. Variation of the calculated band gap energy of RS $Mg_xCd_{1-x}O$ ternaries, using (LDA) and (TB-mBJ) approaches compared to available theoretical data.

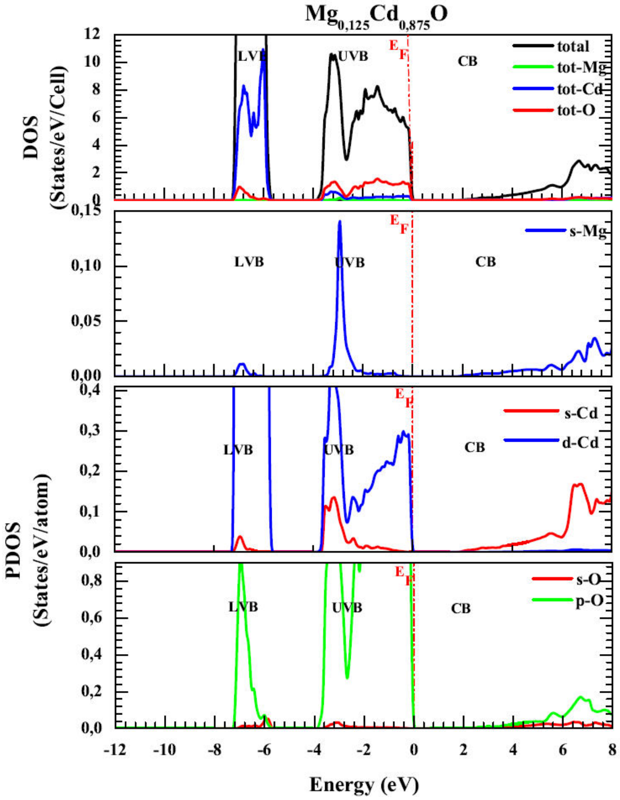

FIGURE 7. Total and partial density of states calculated for RS $Mg_{0.125}Cd_{0.875}O$ using (TB-mBJ) approach.

lated using the (TB-mBJ) approach. The profiles of (TDOS) and (PDOS) profiles are quite similar of $Mg_xCd_{1-x}O$ ternaries for all Mg concentrations, with light differences in the details. Thus, as prototypes, we plotted only the (TB-mBJ) results for RS $Mg_{0.125}Cd_{0.875}O$, RS $Mg_{0.500}Cd_{0.500}O$ and RS $Mg_{0.875}Cd_{0.125}O$ Figs. 6, 7, 8 and 9, respectively. Maximum valence band (VBmax) was placed on the zero-energy Fermi level (E_F). We have divided the electronic states of RS $Mg_xCd_{1-x}O$ ternary in three regions: the lower valence band (LVB) ranging from -7.50 eV to -7.70 eV, upper valence band (UVB) ranging from -4.50 eV to E_F (level Fermi) and conduction band (CB).the second region. The first region (LVB) shows a strong contribution from Cd (d) orbitals, with small participation of O (s,p), Mg (s) and Cd (s) orbitals. This small participation increases with magnesium concentration, but remains low in general compared with the dominance of Cd (d) orbitals. The second region (UVB) is mainly dominated by O (p) with little participation by Mg (s), Cd (s,d) and O (s) orbitals. The conduction band (CB) is composed

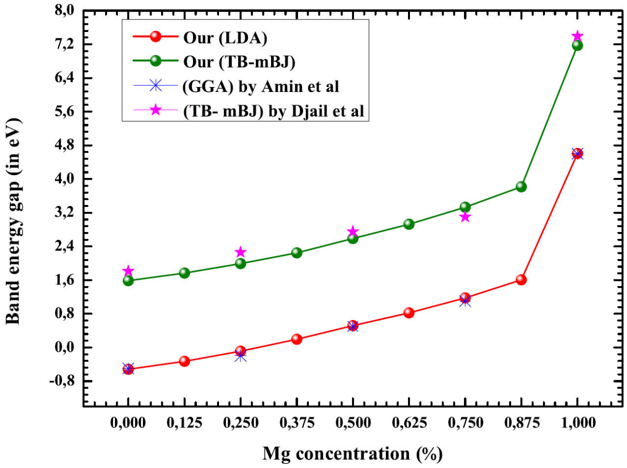

FIGURE 8. Total and partial density of states calculated for RS $Mg_{0.500}Cd_{0.500}O$ using (TB-mBJ) approach.

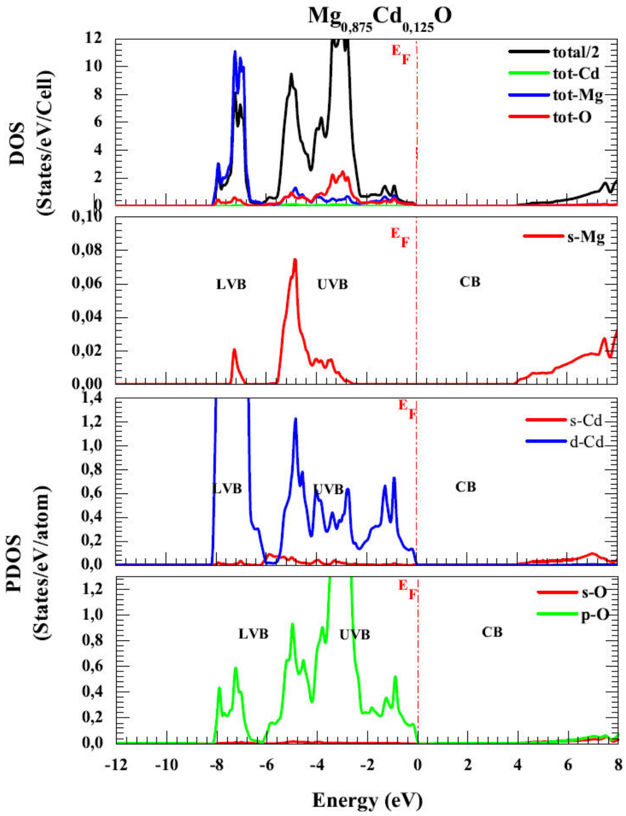

FIGURE 9. Total and partial density of states calculated for RS $Mg_{0.875}Cd_{0.125}O$ using (TB-mBJ) approach.

of Mg (s), Cd (s,d) and O (s,p). From the results, it was observed that when Mg atoms are added, the conduction band minimum ($CB_{\min}$) moves to higher energy, which leads to an increase in the band gap value.

3.3. Optical properties

The optical properties of materials largely verify its response to electromagnetic events. An extensive analysis of these properties was conducted to explore the potential of the compounds for optoelectronic and photovoltaic devices. The dielectric function can be used to describe the optical properties of the material, reflecting the response to light. The dielectric function is a complex function and is given by [15, 44].

$$\varepsilon(\omega) = \varepsilon_1(\omega) + i\varepsilon_2(\omega), \tag{6}$$

where, $\varepsilon_1(\omega)$ is the real part of the complex dielectric function which represents the energy at which electrons are excited while $\varepsilon_2(\omega)$ is the imaginary part of $\varepsilon(\omega)$ which represents the absorption at specific wavelengths [45]. $\varepsilon_1(\omega)$ can be derived from $\varepsilon_2(\omega)$ of the dielectric function through the Kramers-Kronig relationship [15]. Both parts are given by the following equations [15, 44]:

$$\varepsilon_2(\omega) = \left(\frac{4\pi^2 e^2}{m^2\omega^2}\right) \sum_{ij} \int \langle i|M|j\rangle^2 f_i(1-i)\delta \times (E_f - E_i - \omega)\, d^3k, \tag{7}$$

$$\varepsilon_1(\omega) = 1 + \frac{\pi}{2} p \int_0^{\infty} \frac{\omega' \varepsilon_2(\omega')}{\omega'^2 - \omega^2} d\omega'. \tag{8}$$

In Eq. (7), ω present the frequency of the incident photon and M, f_i and e are the dipole matrix, the Fermi distribution function and the electric charge, respectively. In Eq. (8), p is the principal of the integral value. In addition, other important optical parameters, including refractive index $n(\omega)$, the extinction coefficient $k(\omega)$, optical conductivity $\sigma(\omega)$ and absorption coefficient $\alpha(\omega)$ and reflectivity $R(\omega)$ can be calculated from the two parts $\varepsilon_1(\omega)$ and $\varepsilon_2(\omega)$ [44]. These optical parameters are defined by the following relationships [15,46].

$$n(\omega) = \sqrt{\frac{\left(\varepsilon_1^2(\omega) + \varepsilon_2^2(\omega)\right)^{\frac{1}{2}} + \varepsilon_1(\omega)}{2}}, \tag{9}$$

$$k(\omega) = \sqrt{\frac{\left(\varepsilon_1^2(\omega) + \varepsilon_2^2(\omega)\right)^{\frac{1}{2}} - \varepsilon_1(\omega)}{2}}, \tag{10}$$

$$\sigma(\omega) = \frac{i\omega}{4\pi}\varepsilon(\omega). \tag{11}$$

The absorption coefficient, $\alpha(\omega)$, is proportional to the extinction coefficient and can be given by [47]:

$$\alpha(\omega) = \frac{4\pi}{\lambda} k(\omega). \tag{12}$$

Here, λ is the wavelength of light in vacuum. The reflectivity $R(\omega)$ of material at normal incidence can given by the following equation [47]:

$$R(\omega) = \frac{\left(n(\omega) - 1\right)^2 \left(k(\omega)\right)^2}{\left(n(\omega) + 1\right)^2 \left(k(\omega)\right)^2}. \tag{13}$$

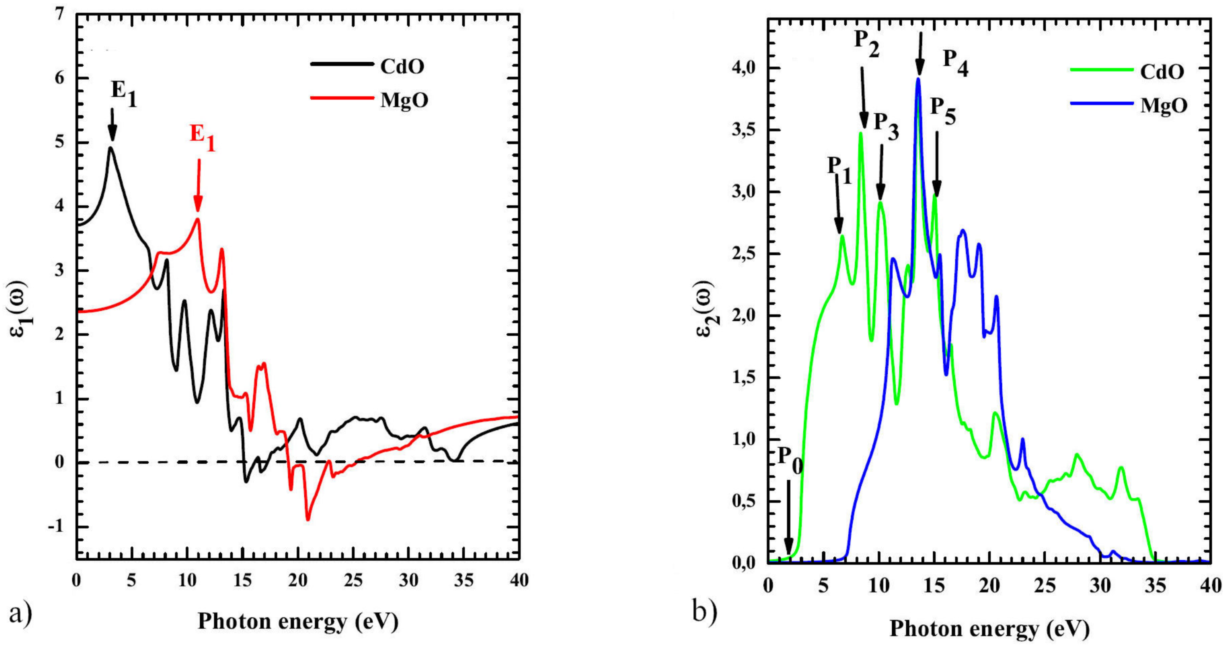

FIGURE 10. a) Real and b) imaginary parts of the dielectric function of RS CdO and RS MgO binaries as function of energy photon with (TB-mBJ) approach.

TABLE III. Static dielectric constant $\varepsilon_1(0)$, E_1 (in eV), and static refractive index $n(0)$ of RS Mg$_x$Cd$_{1-x}$O ternary alloys, with (TB-mBJ) approach.

Compound		This work	Theoretical results			
	$\varepsilon_1(0)$	E_1	$n(0)$	$\varepsilon_1(0)$		$n(0)$
CdO	3.7095	1.9260	1.9260	4 [9]	3.78 [10]	
Mg$_{0.125}$Cd$_{0.875}$O	3.5484	1.8837	1.8837			
Mg$_{0.250}$Cd$_{0.750}$O	3.3801	1.8385	1.8385	3.5 [9]	3.30 [10]	
Mg$_{0.375}$Cd$_{0.625}$O	3.2150	1.7930	1.7930			
Mg$_{0.500}$Cd$_{0.500}$O	3.0480	1.7458	1.7458	3.1 [9]	2.98 [10]	
Mg$_{0.625}$Cd$_{0.375}$O	2.8792	1.6968	1.6968			
Mg$_{0.750}$Cd$_{0.250}$O	2.7059	1.6449	1.6449	2.7 [9]	2.621 [10]	
Mg$_{0.875}$Cd$_{0.125}$O	2.5269	1.5896	1.5896			
MgO	2.3568	1.5352	1.5352	3.1 [9]	2.45 [10]	1.5 [10]

To calculate the optic properties, the program of Abt 1994 and Draxl et Sofo [48, 49] integrated in the Wien2k code is utilized. Optical properties of Mg$_x$Cd$_{1-x}$O ternary alloys, in rock salt phase, are studied by using our (TB- mBJ) results for $1 \leq x \leq 0$. For computational details, the half-width Lorentzian broadening was set to 0.1 eV. And, we increased the number of points in the irreducible part of the Brillouin zone (BZ) to 196 k because the computation of optical properties requires a dense mesh of eigenvalues and their corresponding eigenvectors [33]. To our knowledge, there are no experimental data regarding the optical properties of Mg$_x$Cd$_{1-x}$O ternary alloys, in rock salt phase.

3.3.1. *Complex dielectric function*

Figure 10 illustrates the real and imagery parts of $\varepsilon(\omega)$ function calculated within the (TB- mBJ) scheme of binaries (CdO and MgO) in rock salt structure, for radiation up to 40 eV. The real part $\varepsilon_1(\omega)$ is characterized by the static dielectric constant $\varepsilon_1(0)$, which can be obtained at zero irradiation frequency. The calculated $\varepsilon_1(0)$'s value with (TB-mBJ) approach of CdO and MgO binary compounds are found to be 2.903 and 1.551, respectively. Figure 10a) shows that the $\varepsilon_1(\omega)$'s spectra for CdO presents several maximum peaks at values of 2.237, 1.930 and 1.654 which are localized at 3.074 eV, 8.343 eV, and 13.256 eV, respectively. In the case of Mgo, the values of these maximums are 2.014, 1.985 and 1.487 and they are located at 11.138 eV, 13.212 eV and 17.171 eV, respectively. Table III illustrates our obtained $\varepsilon_1(0)$'s values of RS Mg$_x$Cd$_{1-x}$O ternary alloys. The results shows that $\varepsilon_1(0)$'s values decreases with the increase of Mg concentration. Figure 11a) shows $\varepsilon_1(\omega)$'s spectra as a function of photon energy for RS Mg$_x$Cd$_{1-x}$O ternary alloys, for ($x = 0.125$, 0.500 and 0.875), calculated using (TB-mBJ) approach. We observed that the magnitude of $\varepsilon_1(\omega)$ increases with energy for all ternary alloys and reaches its maximum at E1. This is presented in Fig. 14, where it can be observed that maxima shift to higher energies and decrease with increasing Mg concentration. $\varepsilon_2(\omega)$'s spectra as a function of photon energy for RS Mg$_x$Cd$_{1-x}$O ternary alloys, for ($0.125 \leq x \leq 0.875$), calculated using (TB-mBJ) approach are shown in Fig. 11b) along with the principal peaks (P_0, P_1, P_2, P_3, P_4 and P_5). These principal peaks denote the largest of energy transitions (optical transitions). The threshold energy (P_0) of the $\varepsilon_2(\omega)$ for Mg$_x$Cd$_{1-x}$O ternary alloys as a function of Mg concentration are presented in Fig. 14. These peaks are mainly due to the optical transition ($M_v - \Gamma_c$). We note that both principal peaks (P_0 and P_1) move to higher energies and their magnitude reduce with increase of Mg concentration. While is observed that P_3, P_4 and P_5 shift towards lower energies and peak heights, increasing with increase of Mg concentration.

3.3.2. *Refractive index*

The spectra of refractive index $n(\omega)$ as a function of photon energy for binaries (RS CdO and RS MgO) and RS Mg$_x$Cd$_{1-x}$O are displayed in Fig. 12a) and 13a) , respectively. The calculated results of static refractive index, $n(0)$, in RS Mg$_x$Cd$_{1-x}$O ternary alloys for ($0 \leq x \leq 1$) are given in Table III. From the results, $n(0)$'s values for the two binaries (RS CdO and RS MgO) are 1.926 and 1.5352 respectively. However, these calculated values are in reasonable agreement with those reported in Refs. [9, 10]. The variation of the refractive index $n(x)$ as a function of the Mg concentration x ($0 \leq x \leq 1$) is reported in Fig. 14 and adjusted by a polynomial equation. From the curve, we remarked that the value of $n(x)$ decreases with increasing Mg concentration and deviates from Vegard's law with a small bowing parameter equal to -0.06117. The result of the fit is given as follows:

$$n(\omega) = 1.9256 - 0.3293x - 0.06117x^2. \qquad (14)$$

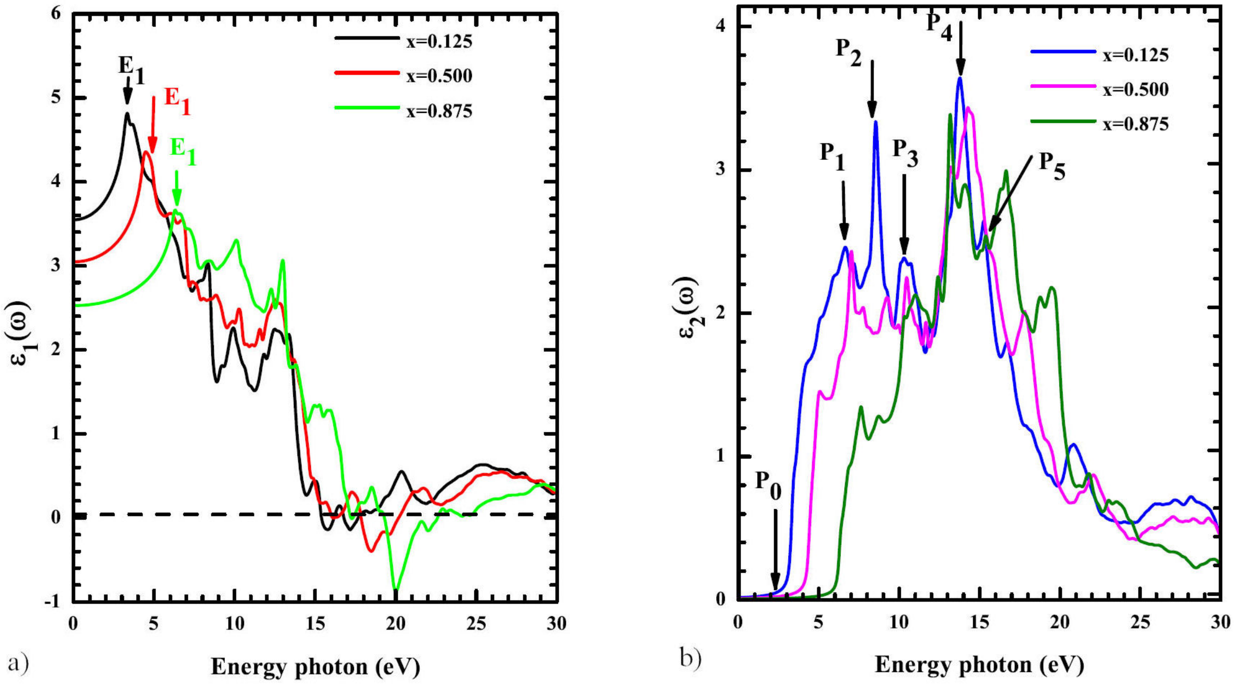

FIGURE 11. a) Real and b) imaginary parts of the dielectric function of RS $Mg_xCd_{1-x}O$ ternaries as function of energy photon with (TB-mBJ) approach.

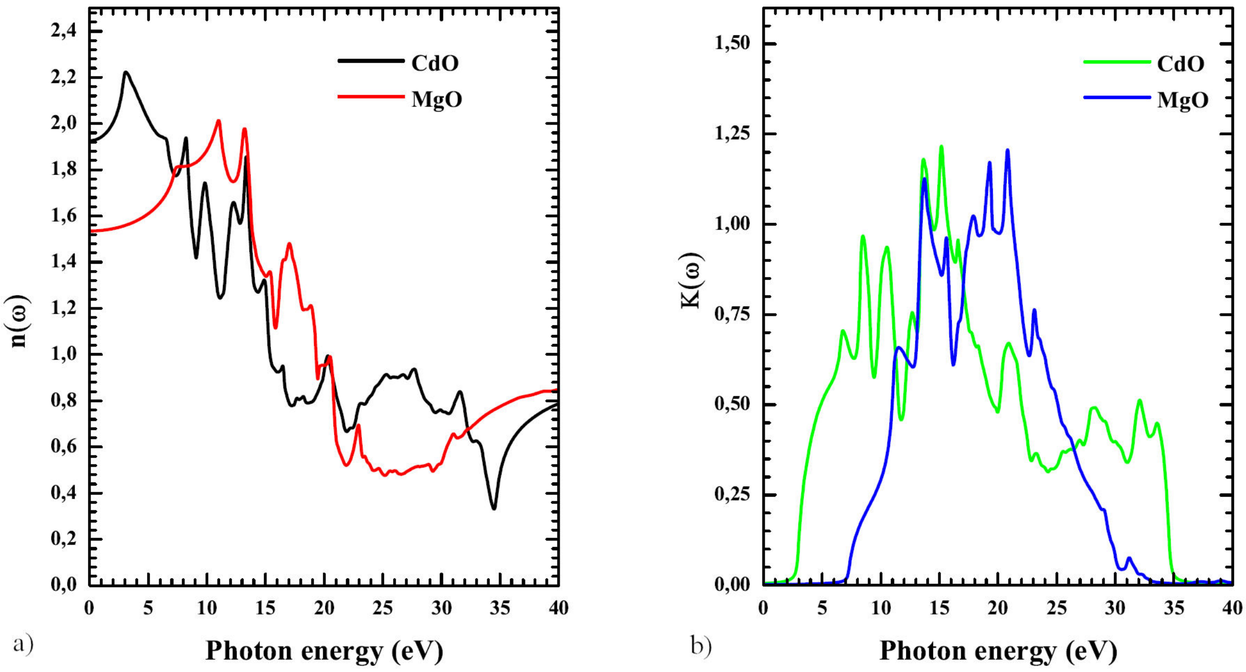

FIGURE 12. a) Refractive index $n(\omega)$ and b) extinction coefficient $k(\omega)$ of RS CdO and RS MgO binaries as function of energy photon with (TB-mBJ) approach.

From Fig. 13a), we observed that $n(\omega)$ increases with increasing photon energy and reaches an upper limit of 2.209 at 3.074 eV for RS CdO and 2.007 at 10.996 eV for RS MgO. After these maxima, $n(\omega)$ decreases with some smaller peaks. Extinction coefficient $k(\omega)$, as a function of photon energy, for binaries and ternaries are shown in Figs. 11b) and 13b), respectively. From these figures, we observed that $k(\omega)$ follows closely to the imaginary part $\varepsilon_2(\omega)$ and describe some sharp peaks that are located in the energy range from 5.351 ± 1.869 eV to 31.143 ± 2.76 eV.

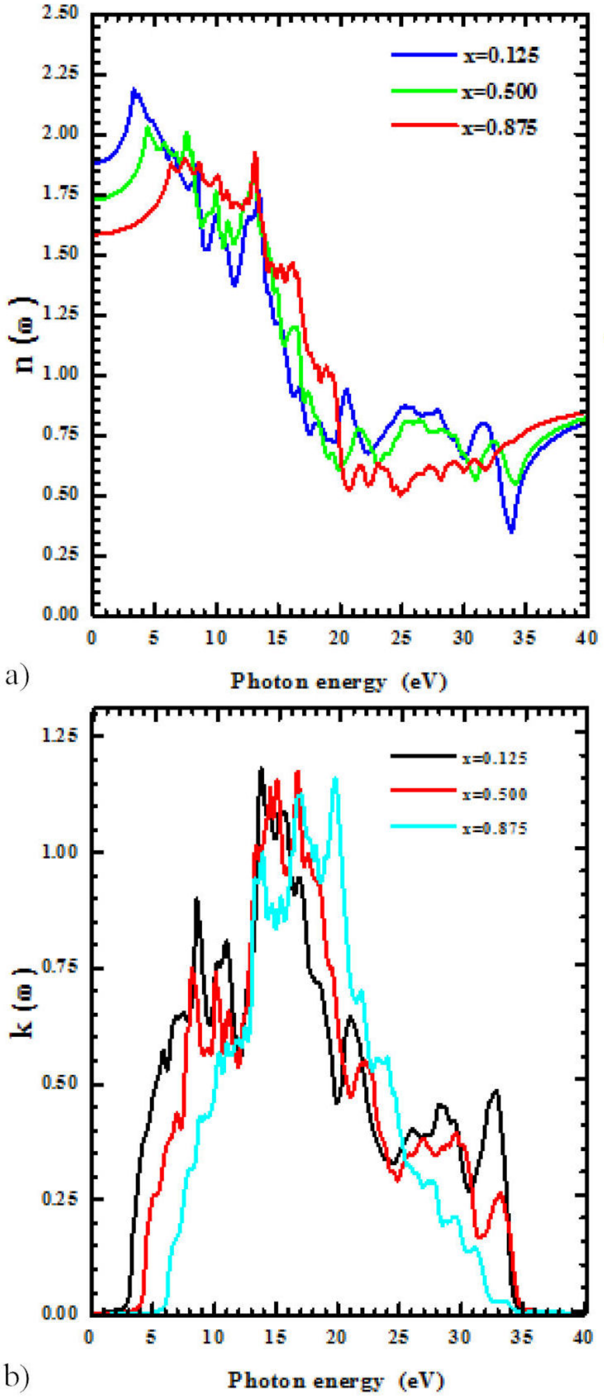

a)

b)

FIGURE 13. a) Refractive index $n(\omega)$ and b) extinction coefficient $k(\omega)$ of RS $Mg_xCd_{1-x}O$ ternaries as function of energy photon with (TB-mBJ) approach.

3.3.3. *Absorption coefficient*

It is well known that the absorption coefficient, $\alpha(\omega)$, reveals the depth of penetration of light into the material [45] and describes the relative decrease in the intensity of incident radiation as it passes through this material. The absorption coefficient spectra of RS CdO and RS MgO binaries as a function of photon energy are displayed in Fig. 15a). As depicted in this figure, the absorption edge begins approximately at 2.525 eV and 6880 eV for RS CdO and RS MgO, respectively. From the results, we observed that both binaries are characterized by a broad absorption band located between 8.223 eV and 27.454 eV for RS CdO and 10.863 eV and 23.683 eV for RS MgO. For ternaries alloys, the absorption coefficient spectra as a function of photon energy for ($x = 0.125$, 0.500 and 0.875) are displayed in Fig. 18. From the results, we can observe that the RS $Mg_xCd_{1-x}O$ ternary alloys exhibit strong absorption, $\alpha(\omega) \geq 25.10^4$ cm^{-1}, in the energy range of 8.965 ± 1.125 eV -32.085 ± 1.969 eV. This indicates that the electrons are accelerated from the valence band to the conduction band. And, these results show that that the ternaries are promising candidate for ultraviolet photoelectronic devices.

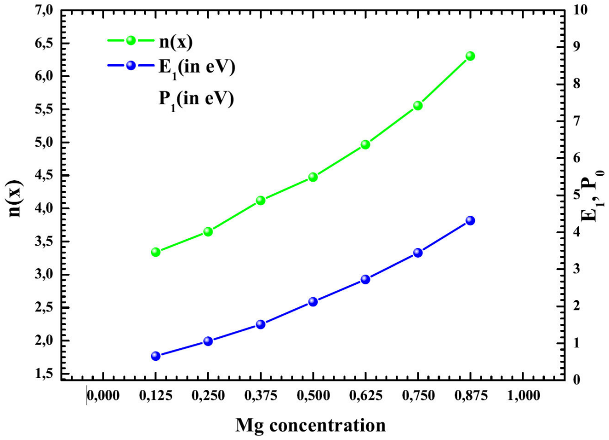

FIGURE 14. Variation of refractive index, $n(0)$, as a function of magnesium concentration for RS $Mg_xCd_{1-x}O$ ternary alloys.

3.3.4. *Optical conductivity*

In Figs. 15b) and 17, we present the spectra of optical conductivity $\sigma(\omega)$ for binaries (RS CdO and RS MgO) and RS $Mg_xCd_{1-x}O$ ternaries as function photon energy. According to these figures, we observe that the optical conductivity of binaries and ternaries $\sigma(\omega)$ starts from their corresponding band gap values. We also notice that the $\sigma(\omega)$ curves contain multiple peaks, which vary depending on the energy band gap. The maximum of optical conductivity is observed in the energy range 4.220-34.198 eV and 9.122-27.788 eV for RS CdO and RS MgO, respectively. In the case of RS $Mg_xCd_{1-x}O$ ternary alloys, it is also observed that the $\sigma(\omega)$ curves exhibit several peaks that vary depending on the energy band gap. From the curves shown in Fig. 17, we observe that optical conductivity values greater than $10^3\Omega^{-1}$ ($\sigma(\omega) \geq 10^3\Omega^{-1}$) lie in the photon energy ranging from 8.964 ± 1.236 eV to 32.029 ± 2.025 eV. Therefore, the presence of high optical conductivities within the UV spectrum underscores the suitability of these materials for optoelectronic applications, indicating their utility in this technology domain.

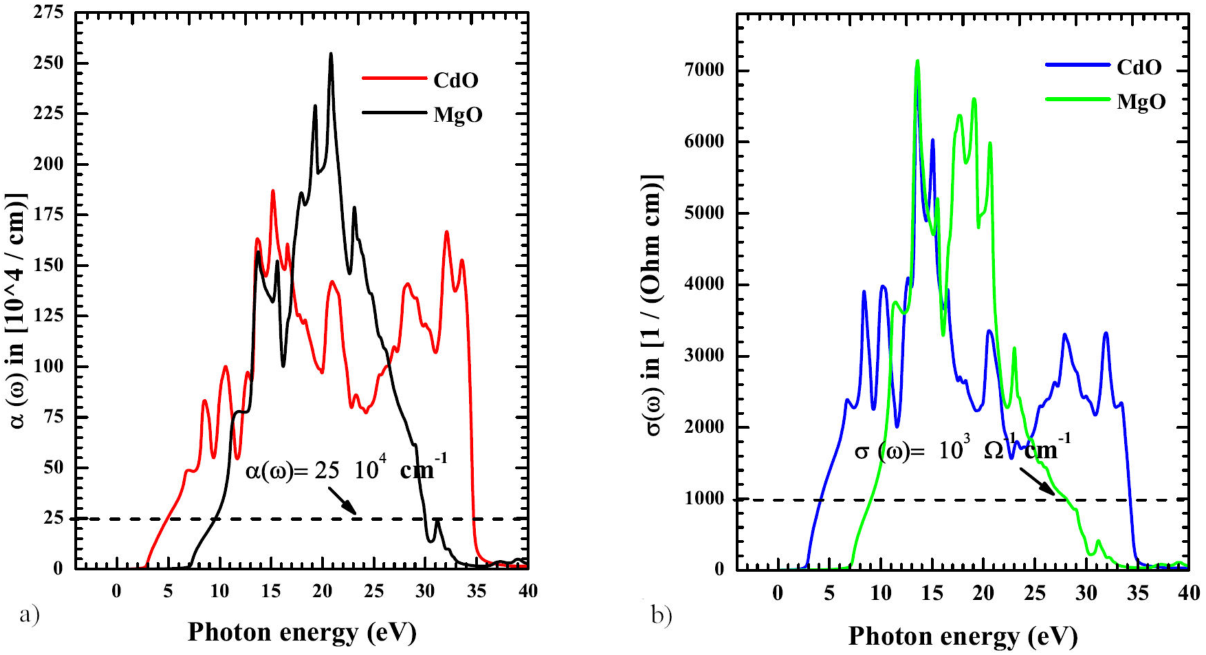

FIGURE 15. a) Absorption coefficient $\alpha(\omega)$ and b) optical conductivity $\sigma(\omega)$ of RS CdO and RS MgO binaries as function of photo energy with (TB-mBJ) approach.

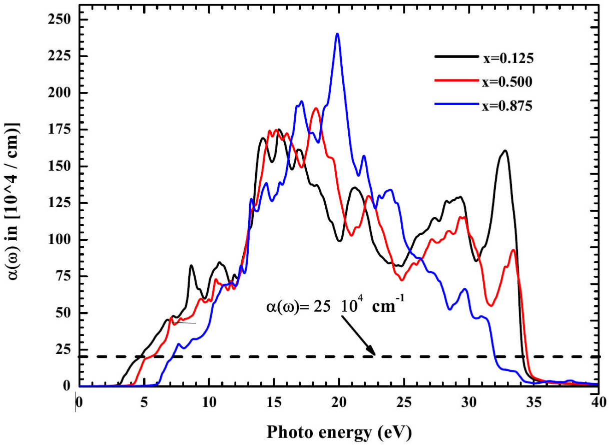

FIGURE 16. Absorption coefficient $\alpha(\omega)$ of RS $Mg_xCd_{1-x}O$ ternaries as function of photo energy with (TB-mBJ) approach.

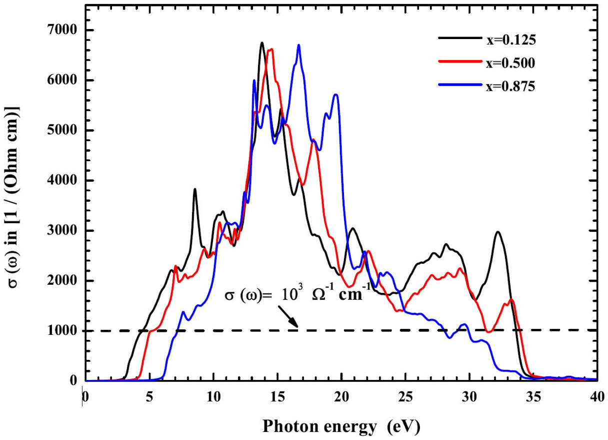

FIGURE 17. Optical conductivity $\sigma(\omega)$ of RS $Mg_xCd_{1-x}O$ ternaries as function of photo energy with (TB-mBJ) approach.

4. Conclusion

The structural and optoelectronic properties of CdO and MgO binary compounds and their $Mg_xCd_{1-x}O$ ternary alloys in rock salt phase were investigated. The (GGA-PBEsol) approximation was used to calculate the structural properties including lattice parameter (a) and bulk modulus (B). The obtained results are reasonably consistent with existing data in the literature. We found that the lattice parameter $(a(x))$ of $Mg_xCd_{1-x}O$ decreases with magnesium composition (x) while its bulk modulus $(B(x))$ increases. Furthermore, we observed that both parameters (a and B) of RS $Mg_xCd_{1-x}O$ alloys can be controlled by adjusting the magnesium composition. In order to examine the electronic properties, we have used (LDA) approach and the modified Becke Johnson potential (TB-mBJ). It is found that the calculated values of band gap using the (TB-mBJ) for the two binaries (RS CdO and RS MgO) are in good agreement with the experimental data. And also, our calculations show that the RS CdO binary has an indirect band gap along $(L-\Gamma)$ while RS MgO has a direct band gap along $(\Gamma-\Gamma)$. In the case of ternaries, calculations show that the maximum of valence band $(VB_{\max})$ and minimum of conduction band $(CB_{\min})$ are located at points R and Γ, respectively, which gives an indirect band gap for all selected concentration x $(0.125 \leq x \leq 0.875)$. It is also noticed that the band gap value (E_g) of RS $Mg_xCd_{1-x}O$ ternary alloys vary almost linearly with the Mg composition and show a bowing parameter equal to 0.951 eV and 1.561 eV, according to the (LDA) and (TB-mBJ) approaches, respectively. Based on our (TB-mBJ) results, we have predicted and discussed in details the optical properties such as complex dielectric function, refractive index, extinction coefficient, absorption coefficient, and optical conductivity of Mg$_x$Cd$_{1-x}$O ternary alloys and their binaries. The obtained optical values for binaries and ternaries show good agreement with existing data. The results signify that our studied ternary alloys are attractive materials for ultraviolet photoelectronic devices.

1. D. Liu, H. Zeng, and R. Sa, First-principles study of physical properties of Zn$_{1-x}$Cd$_x$Te, Zn$_{1-x}$Hg$_x$Te, and Cd$_{1-x}$H$_{g-x}$Te ternary alloys, *Chemical Physics*, **565** (2023) 111755, `https://doi.org/10.1016/j.chemphys.2022.111755.`
2. S.-G. Lee, and K.-J. Chang, First-principles study of the structural properties of MgS-, MgSe-, ZnS-, and ZnSe-based superlattices, *Physical Review B*, **52** (1995) 1918, `https://doi.org/10.1103/PhysRevB.52.1918.`
3. K. Li, X. Wang, H. Zeng, R. Sa, and D. Liu, First-principles study of the structural, electronic and optical properties of Zn$_{1-x}$Hg$_x$Se *Physica B: Condensed Matter*, **629** (2022) 413677, `https://doi.org/10.1016/j.physb.2022.413677.`
4. H. Slimani, H. Abid, and M. Benchehima, Prediction of optoelectronic properties for Be$_x$Zn$_y$Cd$_{1-x-y}$Se quaternary alloys: First-principles study, *Optik*, **198** (2019) 163288, `https://doi.org/10.1016/j.ijleo.2019.163288.`
5. K. Benchikh, H. Abid, and M. Benchehima, Electronic and optical properties of ternary alloys Zn$_x$Cd$_{1-x}$S, Zn$_x$Cd$_{1-x}$Se, ZnS$_x$Se$_{1-x}$, Mg$_x$Zn$_{1-x}$Se, *Mater. Sci.-Poland*, **35** (2017) 32, `https://doi.org/10.1515/msp-2017-0005.`
6. W.U. Huynh, J.J. Dittmer, and A.P. Alivisatos, Hybrid Nanorod-Polymer Solar Cells *Science*, **295** (2002) 2425-2427, `DOI:10.1126/science.1069156.`
7. N. Tessler, V. Medvedev, M. Kazes, S. Kan, and U. Banin, Efficient Near-Infrared Polymer Nanocrystal Light-Emitting Diodes, *Science*, **295** (2002) 1506-1508, `DOI:10.1126/science.1068153.`
8. B. Dabbousi, M. Bawendi, O. Onitsuka, and M. Rubner, Electroluminescence from CdSe quantum-dot/polymer composites, *Applied Physics Letters*, **66** (1995) 1316, `https://doi.org/10.1016/j.ijleo.2019.163288.`
9. B. Amin *et al.*, Generalized gradient calculations of structural, electronic and optical properties of Mg$_x$Cd$_{1-x}$O oxides, *Journal of alloys and compounds*, **493** (2010) 212-218, `https://doi.org/10.1016/j.jallcom.2009.12.057`
10. S. Djaili, M. Hachi, B. Lagoun, T. Smain, A. Amor, and K. Souleh, First-principles study of electronic and optical properties of Cd$_x$Mg$_{1-x}$O alloys, TB-mBJ calculations, *Optical and Quantum Electronics*, **55** (2023) 297, `https://doi.org/10.1007/s11082-023-04612-3.`
11. B. Amrani, R. Ahmed, and F.E.H. Hassan, Structural, electronic and thermodynamic properties of wide band gap Mg$_x$Zn$_{1-x}$O alloy, *Computational Materials Science*, **40** (2007) 66-72, `https://doi.org/10.1016/j.commatsci.2006.11.001.`
12. R. Whited, C.J. Flaten, and W. Walker, Exciton thermoreflectance of MgO and CaO, *Solid state communications*, **13** (1973) 1903-1905, `https://doi.org/10.1016/0038-1098(73)90754-0.`
13. D. Roessler and W. Walker, Electronic Spectrum and Ultraviolet Optical Properties of Crystalline MgO, *Physical Review*, **159** (1967) 733, `https://doi.org/10.1103/PhysRev.159.733.`
14. J. Kocka and C. Konak, The Structure of the Indirect Absorption Edge of CdO, *physica status solidi (b)*, **43** (1971) 731-738, `https://doi.org/10.1002/pssb.2220430234.`
15. S. Adachi, Properties of semiconductor alloys: group-IV, III-V and II-VI semiconductors, (John Wiley & Sons, 2009).
16. L. He, M. Tang, M. Zeng, X. Zhou, W. Zhu, and F. Liu, First-principles calculations of optical properties of perfect and defective MgO crystals at high pressure, *Physica B: Condensed Matter*, **410** (2013) 137-140, `https://doi.org/10.1016/j.physb.2012.10.038.`
17. J. Li, X. Zhou, and J. Li, A time-resolved single-pass technique for measuring optical absorption coefficients of window materials under 100 GPa shock pressures, *Review of Scientific Instruments*, **79** (2008), `https://doi.org/10.1063/1.3046279.`
18. J.H. Lee *et al.*, Hydration behavior of MgO single crystals and thin films, *Journal of materials research*, **18** (2003) 2895-2903, `https://doi.org/10.1557/JMR.2003.0404.`
19. H. Kohler, Optical properties and energy-band structure of CdO, *Solid state communications*, **11** (1972) 1687-1690, `https://doi.org/10.1016/0038-1098(72)90772-7.`
20. M. Labidi, S. Labidi, F.E.H. Hassan, M. Boudjendlia, and R. Bensalem, Structural, electronic and thermodynamic properties of Sr$_x$Cd$_{1-x}$O: A first-principles study, *Materials Science in Semiconductor Processing*, **16** (2013) 1853-1858. `https://doi.org/10.1016/j.mssp.2013.07.011`
21. F. Henari and A. Dakhel, Linear and nonlinear optical properties of hydrogenated CdO thin films, *Laser physics*, **18** (2008) 1557-1561, `https://doi.org/10.1134/S1054660X08120281.`
22. D.O. Scanlon, A. Walsh, B.J. Morgan, M. Nolan, J. Fearon, and G.W. Watson, Surface Sensitivity in Lithium-Doping of MgO: A Density Functional Theory Study with Correction for on-Site Coulomb Interactions, *The Journal of Physical Chemistry C*, **111** (2007) 7971-7979, `https://doi.org/10.1021/jp070200y.`
23. U. Paliwal, T. Bredow, and K. Joshi, Structural properties of Mg$_x$Cd$_{1-x}$O alloys, AIP Conference Proceedings, *American Institute of Physics*, **1447** (2012) 1037, `https://doi.org/10.1063/1.4710360.`

24. K. Joshi, U. Paliwal, K. Galav, D. Trivedi, and T. Bredow, Study of $\mathrm{Mg}_x\mathrm{Cd}_{1-x}\mathrm{O}$ applying density functional theory: Stability, structural phase transition and electronic properties, *Journal of Solid State Chemistry,* **204** (2013) 367-372, `https://doi.org/10.1016/j.jssc.2013.06.015`.
25. Z. Wu, R.E. Cohen, More accurate generalized gradient approximation for solids, *Physical Review B,* **73** (2006) 235116, `https://doi.org/10.1103/PhysRevB.73.235116`.
26. J. Munir *et al.*, Spin-polarized electromagnetic and optical response of full-Heusler $\mathrm{Co_2VZ}$ (Z=Al, Be) alloys for spintronic application, *The European Physical Journal Plus*, **136** (2021) 1-18, `https://doi.org/10.1140/epjp/s13360-021-01968-x`.
27. D. Koelling and B. Harmon, A technique for relativistic spinpolarised calculations, *Journal of Physics C: Solid State Physics,* **10** (1977) 3107, `DOI10.1088/0022-3719/10/16/019`.
28. J.P. Perdew *et al.*, Restoring the Density-Gradient Expansion for Exchange in Solids and Surfaces, *Physical Review Letters,* **100** (2008) 136406, `https://doi.org/10.1103/PhysRevLett.100.136406`.
29. W. Kohn, and L. Sham, Self-Consistent Equations Including Exchange and Correlation Effects, *Phys. Rev. A,* **140** (1965) 1133, `https://doi.org/10.1103/PhysRev.140.A1133`.
30. D. Ceperley and B. Alder, Ground State of the Electron Gas by a Stochastic Method, *Rev. Lett,* **45** (1980) 566, `https://doi.org/10.1103/PhysRevLett.45.566`.
31. X. Li *et al.*, First-principles investigations of structural, electronic, optical and thermodynamic properties of $\mathrm{Cd}_x\mathrm{Mg}_{1-x}\mathrm{S}$ alloys, *Computational Materials Science,* **101** (2015) 242-247, `https://doi.org/10.1016/j.commatsci.2015.02.002`
32. P. Hohenberg and W. Kohn, Inhomogeneous Electron Gas, *Phys. Rev. B,* **136** (1964) 864, `https://doi.org/10.1103/PhysRev.136.B864`.
33. P. Blaha, K. Schwarz, G. Madsen, D. Kvasnicka, and J. Luitz, An Augmented Plane Wave+ Local Orbitals Program for Calculating Crystal Properties (Institut Für Physikalische und Theoretische Chemie: Vienna, Austria, 2001).
34. A. Zunger, S.-H. Wei, L. Ferreira, and J.E. Bernard, Special quasirandom structures, *Physical review letters*, **65** (1990) 353, `https://doi.org/10.1103/PhysRevLett.65.353`.
35. I. Vurgaftman, J. Meyer, and L.R. Ram-Mohan, Band parameters for III-V compound semiconductors and their alloys, *Journal of applied physics,* **89** (2001) 5815-5875, `https://doi.org/10.1063/1.1368156`.
36. F. Murnaghan, The Compressibility of Media under Extreme Pressures, *PNAS,* **30** (1944) 244, `https://doi.org/10.1073/pnas.30.9.244`.
37. J. Zhang, Room-temperature compressibilities of MnO and CdO: further examination of the role of cation type in bulk modulus systematics, *Physics and Chemistry of Minerals,* **26** (1999) 644-648, `https://doi.org/10.1007/s002690050229`.
38. H. Mao and P. Bell, Equations of state of MgO and ε Fe under static pressure conditions, *Journal of Geophysical Research: Solid Earth,* **84** (1979) 4533-4536, `https://doi.org/10.1029/JB084iB09p04533`.
39. M.L. Cohen, Calculation of bulk moduli of diamond and zincblende solids, *Physical Review B,* **32** (1985) 7988, `https://doi.org/10.1103/PhysRevB.32.7988`.
40. S. Hosseini, T. Movlarooy and A. Kompany, First-principle calculations of the cohesive energy and the electronic properties of $\mathrm{PbTiO_3}$, *Physica B: Condensed Matter,* **391** (2007) 316-321, `https://doi.org/10.1016/j.physb.2006.10.013`.
41. F. Tran and P. Blaha, Accurate Band Gaps of Semiconductors and Insulators with a Semilocal Exchange-Correlation Potential, *Physical review letters,* **102** (2009) 226401, `https://doi.org/10.1103/PhysRevLett.102.226401`.
42. M. Benchehima, M.H. Hachemi and H. Abid, Theoretical studies of optoelectronic properties of $\mathrm{AlP}_{1-x}\mathrm{Bi}_x$ ternaries: Promising light sources for fiber optic communications, *Radiation Physics and Chemistry,* **202** (2023) 110591, `https://doi.org/10.1016/j.radphyschem.2022.110591`.
43. M. Benchehima and H. Abid, Electronic and optical properties of $\mathrm{Al}_x\mathrm{GayIn}_{1-x-y}\mathrm{As}$ quaternary alloys with and without relaxation lattice matched to InP for laser applications: First-principles study, *Optik,* 127 (2016) 6541-6558, `https://doi.org/10.1016/j.ijleo.2016.04.092`.
44. M. Tehami, M. Benchehima, D. Ameur and H. Abid, First-principle study of the optoelectronic properties of $\mathrm{Ga}_x\mathrm{In}_{1-x}\mathrm{Bi}_y\mathrm{P}_{1-y}$ quaternary alloys lattice-matched to InP for telecommunication applications, *Canadian Journal of Physics*, **101** (2023) 471-483, `https://doi.org/10.1139/cjp-2022-0331`.
45. Q. Rafiq *et al.*, Investigation of structural, electrical, magnetic, and optical properties of Cu (111) and the impact of Ag adatoms adsorption: A density functional theory study, *International Journal of Electrochemical Science,* **19** (2024) 100603, `https://doi.org/10.1016/j.ijoes.2024.100603`.
46. K. Benchikh, M. Benchehima, H. Abid, and A. Chaouche, Prediction of electronic and optical properties for $\mathrm{Zn}_{1-x}\mathrm{Cd}_x\mathrm{Se}_y\mathrm{Te}_{1-y}$ quaternary alloys: First-principles study, *Rev. Mex Fis*. **67** (2021), `https://doi.org/10.31349/revmexfis.67.041001`.
47. M. Benchehima and H. Abid, Effects of phosphorus incorporation on the structural and optoelectronic properties of BSb binary compound: A first principle investigation, *Computational Condensed Matter,* **14** (2018) 114-124, `https://doi.org/10.1016/j.cocom.2018.01.011`.
48. R. Abt, C. Ambrosch-Draxl and P. Knoll, Optical response of high temperature superconductors by full potential LAPW band structure calculations, *Physica B: Condensed Matter,* **194** (1994) 1451, `https://doi.org/10.1016/0921-4526(94)91225-4`.
49. C. Ambrosch-Draxl and J.O. Sofo, Linear optical properties of solids within the full-potential linearized augmented planewave method, *Computer physics communications*, **175** (2006) 1-14, `https://doi.org/10.1016/j.cpc.2006.03.005`.